Demonstration of moleculelike modes of doubly excited states in hyperspherical coordinates

S. Watanabe
Observatoire de-Paris-Meudon, 92190 Meudon, France

C. D. Lin
Department of Physics, Cardwell Hall, Kansas State University, Manhattan, Kansas 66506
(Received 22 July 1985)

The moleculelike normal modes formed by a pair of correlated electrons are examined through analysis of their wave functions in a body frame of the atom. The quantum numbers used by Lin for the classification of doubly excited states are reinterpreted from the body-frame viewpoint, and their connections with the rovibrator model of Herrick and Kellman are identified. This analysis also sheds light on the limitations of the rovibrator model of two correlated electrons. Because electrons are light and are not localized like atoms in a molecule, departure from the rovibrator picture grows rapidly as the rovibrational energy rises. Other limitations of the rovibrator model of doubly excited states stem from the following facts: (1) the dominant contribution to the rotational constant comes from the bielectronic repulsion instead of the kinetic energy; (2) the rotational contraction and T doubling result from atomic shell structure. We also include a brief discussion of the correspondence between the molecular stretching modes and the radial correlations of two electrons. The systematics of autoionization widths with respect to the correlation quantum numbers are also considered.

I. INTRODUCTION

The discovery of moleculelike normal modes[1-5] of a pair of electrons in doubly excited states has furnished a new perspective to the study of electron-pair correlations. Under the influence of strong correlation, a pair of electrons perform motion akin to that of a floppy XYX molecule where each X represents an electron and Y the nucleus. This molecular picture was first applied to characterize the angular correlation of intrashell states, namely, states in which the two electrons are roughly at an equal distance from the nucleus. Indeed, the level structure of doubly excited states was found to fit into patterns called supermultiplets[1,2] which regroup intrashell states according to the degree of moleculelike rotational and vibrational excitations. The relative level spacing of intrashell states thus reveals systematic features easily parametrized by a few constants analogous to molecular constants.

The rovibrator energy-level structure was first interpreted in a group-theoretical framework. However, the involved algebra somehow overshadowed the relevance of the model. A more direct "verification" came from the visualization of that portion of the wave function[4,5] which was considered responsible for the moleculelike behavior. In one such model to describe angular correlations the two electrons were assumed to be rigidly placed on concentric spherical surfaces similar to the rigid-bender model.[6] Despite the fictitious constraints, the angular wave functions have the desired behavior, thus providing a first verification of the rovibrator model of doubly excited states.

Along a different line, an extensive investigation of doubly excited states was being carried out by Lin.[7] Relief plots of wave functions in hyperspherical coordinates are used to reveal the nature of different electron correlations. In addition to the angular correlations examined in the rigid-bender model, the importance of radial correlation was emphasized in Lin's classification scheme. Labels $A=+$, $-$ and 0 were introduced for classifying radial correlation patterns.[7(d)] Here the $+$ and $-$ label the antisymmetric stretching modes, used by quantum chemists for describing triatomic molecules (see Sec. III D). Doubly excited states labeled by $A=+$ exhibit in-phase radial oscillation, i.e., the two electrons tend to approach or to move away from the nucleus in phase. Doubly excited states labeled by $A=-$ exhibit out-of-phase radial motion such that when one electron approaches the nucleus, the other tends to move away from it. States with $A=0$ exhibit little radial correlation; they resemble singly excited states since one of the electrons tends to stay far away from the nucleus while the other stays close in, showing no obvious phase relationship. Since the two electrons in the system achieve stability by optimizing radial and angular correlations, the analysis in hyperspherical coordinates provides a complete description of the correlations of doubly excited states.

The hyperspherical viewpoint[7-11] describes electron correlations in terms of the nodal structure of the two-electron wave functions, revealing the relative radial and angular motion of the electron pair. The analysis of correlations is based on the approximate solution of the Schrödinger equation in hyperspherical coordinates. What is the relevance of the rovibrator model of doubly excited states to this approach? One purpose of this paper is to answer this question. Meanwhile, the analysis also explores to what extent the rovibrator model is valid for describing the correlations of doubly excited states.

There are at least two conceptual merits of merging two

different models and viewpoints. First, the hyperspherical method was conceived from the viewpoint of "channels" whereas the group-theoretical consideration stemmed from configuration interaction. The intrashell state, for example, derives from the configuration-interaction viewpoint whereas the hyperspherical method regards it as the lowest resonant state of a channel which possesses in-phase radial correlation ($A=+$) pattern. In the hyperspherical approach, intershell states belonging to the same channel reflect the same correlation pattern. This conceptual continuity is useful if we wish to extend the rovibrator model to deal with dynamical processes involving continua such as photoionization[11] or electron-impact ionization. Another merit of the hyperspherical method in comparison with the more restricted rigid-bender model is that the former incorporates the radial degree of freedom. Thus, for example, the centrifugal distortion[1(a),5] comes out with the correct sign as in the fitting to the molecule-like term formula showing that doubly excited states actually contract as the total angular momentum increases whereas the more restricted rigid-bender model leads to the opposite conclusion (Sec. IV C). The phenomenon of the T doubling similarly comes out with the correct sign owing to the inclusion of the radial degree of freedom (Sec. IV D).

Although there is little doubt about the relevance of associating two-electron normal modes with those of a floppy XYX molecule, some questions remain open at a more quantitative level. For example, what is the nature of the internal axis about which the two electrons rotate? This is a fairly meaningful question in view of the wave nature of electrons. The atom is more like a gas than a solid or a liquid drop so that the concept of a well-defined axis at first sight contradicts the high mobility of electrons. Another question pertains to the rovibrational quantum numbers. The molecular energy term formula presumes that the bending vibrational quantum numbers be well respected in zero order; otherwise higher-order corrections make little sense. How well are these quantum numbers respected?

In this paper we attempt to give certain perspectives to these questions from the hyperspherical viewpoint. It should be emphasized that the character of approximate quantum numbers depends on the particular theoretical framework employed for analysis because of the lack of exact separability of the two-electron problem. Major features of the system, of course, should not differ greatly from one scheme to another if they portray the same reality. The advantage of one scheme over the other thus is its generality and its greater applicability.

Our major objective is to synthesize and extend previous studies by analyzing two-electron wave functions in the body frame of the atom. Our body frame is attached to the axis parallel to the interelectronic axis $\hat{\mathbf{r}}_{12}$ passing through the center of mass. It does not necessarily coincide with that attached to the instantaneous principal axes of inertia. The correspondence of this choice of the body-frame axes with the O(4) theory is described in Sec. II A.

The rest of the paper consists of three sections. Section II presents the procedure of analysis. In Sec. II A, we discuss the meaning of the internal axis of rotation. The correspondence of our body-frame axis to the vector $\mathbf{B}=\mathbf{b}_1-\mathbf{b}_2$ exploited in the O(4) theory[12,13] is also discussed. In Sec. II B we consider the operator $\mathbf{L}\cdot\hat{\mathbf{r}}_{12}$ and introduce a scheme for decomposing an arbitrary wave function into the eigenstates of $\mathbf{L}\cdot\hat{\mathbf{r}}_{12}$. It is shown that each rotational component possesses well-defined symmetry properties under electron exchange. After a brief review of the hyperspherical method and of the labeling scheme in terms of correlation quantum numbers K, T, and A [Refs. 3 and 7(d)] (Sec. III A), we examine the decomposition of hyperspherical wave functions into rotational components in Sec. III B. It is shown that the quantum number T used in the labeling of doubly excited states in Ref. 7(d) is identical to the dominant rotational component of the wave function. Whenever the identification of the dominant rotational component is possible, the label A can be assigned uniquely, its value, $+$ or $-$, depending on T, total spin, and parity of the state [Eq. (14)]. Thus the radial correlation quantum number A is unambiguous only when the dominant rotational component is also unambiguous. States which have nearly equal amplitude in each rotational component do not show clear radial correlation patterns. Accordingly these states are labeled as $A=0$.[7(d)] In order to relate the K, T, and A quantum numbers to the molecule-like modes of doubly excited states, we demonstrate in Secs. III C and III D that the label K relates to the bending vibrational mode, and A to the antisymmetric stretching mode of a triatomic molecule. Section IV is devoted to studying specific features of molecule-like modes and the limitations of associating doubly excited states with these modes. In Sec. IV A the rotational and vibrational constants obtained from the calculated energies are used to test the scaling laws down the isoelectronic sequence. These constants are shown to originate dominantly from the electron-electron interaction rather than from the kinetic energy of the rigid rotor (a reason why the correspondence is no more than analogy). In Sec. IV B we discuss the rotational contraction of doubly excited states by providing qualitative evidence from the analysis of hyperspherical channel functions. We comment on the information about the T doubling provided by the hyperspherical channel functions in Sec. IV C. A brief discussion on the systematics of autoionization widths based on the nature of correlations is given in Sec. V. We conclude in Sec. VI.

II. THE BODY-FRAME ANALYSIS

A. The choice of the axes

In dealing with a highly nonrigid system such as a two-electron atom, the meaning of the body frame at first appears obscure. This obscurity is merely deceptive because the positions of two electrons considered in quantum mechanics are statistical in nature and correspond to the time-averaged effective positions in classical mechanics. In other words, a position vector here represents a point in space through which a bundle of classical trajectories pass but it does not represent the instantaneous po-

sition of the electron moving on a particular trajectory. Let us take a simple example of an electron in the Coulomb field. In this case, time averaging is accomplished by Pauli's substitution

$$\mathbf{r}\rightarrow\frac{3n}{2Z}\mathbf{b}\ , \tag{1}$$

where $\mathbf{b}$ is the Lenz vector. When the effect of the mutual interaction of the electrons is included, the time average of $\mathbf{r}$ departs from Eq. (1), and varies slowly so long as the perturbation is weak. Since we study the eigenfunctions of the two-electron system explicitly, the body frame we consider here is attached to such effective position vectors of the two electrons rather than to their instantaneous positions and evolves slowly under the influence of the interelectronic interaction.

There are many different ways of choosing body-frame axes. In this work, we take the interelectronic axis

$$\hat{\mathbf{r}}_{12}=(\mathbf{r}_1-\mathbf{r}_2)/|\mathbf{r}_1-\mathbf{r}_2| \tag{2}$$

as the internal axis of rotation with the axis passing through the nucleus. There are three reasons for this choice. First, the vector $\mathbf{r}_{12}=\mathbf{r}_1-\mathbf{r}_2$ serves as a measure of the relative orientation and closeness of the electrons' orbits. This choice of the rotational axis separates the degree of freedom in the bending motion from the rotation of the body. Second, this axis is democratic with respect to the exchange of the two electrons. A number of powerful symmetry properties thus follow (Sec. II B). Third, the general behavior of this axis is similar to that of the vector $\mathbf{B}=\mathbf{b}_1-\mathbf{b}_2$ exploited in the O(4) theory of doubly excited states.[12,13] In fact, the substitution of Eq. (1) gives

$$\mathbf{B}=\frac{2}{3}\left[\frac{Z_1}{n_1}\mathbf{r}_{12}+\left[\frac{Z_1}{n_1}-\frac{Z_2}{n_2}\right]\mathbf{r}_2\right]\ . \tag{3}$$

Let us consider the behavior of $\mathbf{B}$ in two limiting cases of interest. One is the intrashell state in which the two electrons have similar average distances, and experience similar degree of screening (i.e., $n_1\approx n_2=n$, $Z_1\approx Z_2=Z$); there $\mathbf{B}\approx(2Z/3n)\mathbf{r}_{12}$. In the other, one electron is far away so that $r_1\gg r_2$ (or $n_1^2/Z_1\gg n_2^2/Z_2$); $\mathbf{B}$ is again proportional to $\mathbf{r}_{12}$ if we ignore terms of order n_2/n_1. Certainly one can choose the more abstract $\hat{\mathbf{B}}$ as the axis of internal rotation, but this choice requires us to know the effective charges Z_1 and Z_2 as well as the principal quantum numbers n_1 and n_2. Since there are no *a priori* values of these parameters when the Kepler orbitals of the electrons are strongly perturbed, the choice of $\hat{\mathbf{B}}$ is not practical for our purposes. The use of $\hat{\mathbf{r}}_{12}$ is thus intended to remove this limitation of $\hat{B}$.

The unit vector $\hat{\mathbf{r}}_{12}$ permits us to separate the body's rotational degree of freedom from the rest. Unfortunately, in doing this, the information on bending vibration conveyed by the length of the vector $\mathbf{r}_{12}$ also becomes removed. As a result, other quantum numbers require separate considerations. We discuss this point later in Secs. IV C and IV D.

Before leaving this section, a few remarks about other choices of body-frame axes are pertinent. For example, if our purpose was oriented toward calculating the body-frame wave functions, we could employ the Eckart frame.[14] In this frame, the coupling between the bending vibration and the Coriolis force is minimized near the equilibrium configuration. If the system were a quasirigid rovibrator, we could use the principal axes of inertia as the rotational axes. However, the manifestation of the moleculelike modes in doubly excited states is somewhat more abstract much as the rotor and vibrator structure in the excitation spectrum of the hydrogen atom in a strong magnetic field.[15] It is the electrons' orbit which exhibits such modes. Similarly, the moleculelike modes in doubly excited states arise presumably from the mutual polarization of the orbits of the two electrons. The exchange symmetry enhances the moleculelike modes by imposing strict constraints on the possible geometry the two-electron orbitals can attain. For these reasons, we have chosen a set of axes adapted to the representation of mutual polarization as well as the exchange symmetry of the electron pair, namely, $\hat{\mathbf{r}}_{12}$ and a pair of vectors orthogonal to $\hat{\mathbf{r}}_{12}$.

B. Decomposition into rotational components

Here we consider the decomposition of an arbitrary two-electron wave function into rotational components and study the symmetry properties of each component under electron exchange. Our body frame is defined by three unit vectors, $\hat{\mathbf{r}}_{12}$, $\hat{\mathbf{t}}=(\hat{\mathbf{r}}_1\times\hat{\mathbf{r}}_2)/|\hat{\mathbf{r}}_1\times\hat{\mathbf{r}}_2|$, and $\hat{\mathbf{s}}=\hat{\mathbf{t}}\times\hat{\mathbf{r}}_{12}$ such that the set $(\hat{\mathbf{s}},\hat{\mathbf{t}},\hat{\mathbf{r}}_{12})$ forms a right-handed system (see Fig. 1). This frame is singular whenever the triangle formed by $\mathbf{r}_1$, $\mathbf{r}_2$, and the origin becomes degenerate. Fortunately, such a singular configuration has measure zero so that it causes no practical difficulty.

Let us denote the Euler angled by $\hat{\Omega}=(\Phi,\Theta,\Psi)$. The transformation from the laboratory frame to the body frame satisfies the following relationship:

$$\mathscr{Y}_{l_1l_2LM}(\hat{\mathbf{r}}_1,\hat{\mathbf{r}}_2)=\sum_Q\mathscr{Y}_{l_1l_2LQ}(\hat{\mathbf{r}}'_1,\hat{\mathbf{r}}'_2)D^{(L)}_{QM}(\hat{\Omega})\ , \tag{4}$$

where $(\hat{\mathbf{r}}_1,\hat{\mathbf{r}}_2)$ are defined in the laboratory frame and $(\hat{\mathbf{r}}'_1,\hat{\mathbf{r}}'_2)$ in the body frame, and $D^{(L)}_{QM}$ is the rotation matrix. By definition,

$$(\mathbf{L}\cdot\hat{\mathbf{r}}_{12})\mathscr{Y}_{l_1l_2LQ}(\hat{\mathbf{r}}'_1,\hat{\mathbf{r}}'_2)=Q\mathscr{Y}_{l_1l_2LQ}(\hat{\mathbf{r}}'_1,\hat{\mathbf{r}}'_2)\ . \tag{5}$$

According to Fig. 2, the polar coordinates of $\hat{\mathbf{r}}'_1$ and $\hat{\mathbf{r}}'_2$ are given by

$$\hat{\mathbf{r}}'_1=(\chi,0)\ ,$$
$$\hat{\mathbf{r}}'_2=(\chi+\theta_{12},0)\ , \tag{6}$$

where

$$\tan\chi=\sin\theta_{12}/(r_1/r_2-\cos\theta_{12})\ . \tag{7}$$

Because χ depends on the ratio of the arm lengths r_1 and r_2 and on the relative angular separation θ_{12}, it is convenient to introduce the hyperspherical coordinates at this stage. We replace the independent-particle radial variables r_1 and r_2 by the size parameter R and the pseudoangle α defined by

$$r_1=R\cos\alpha\ ,$$
$$r_2=R\sin\alpha\ . \tag{8}$$

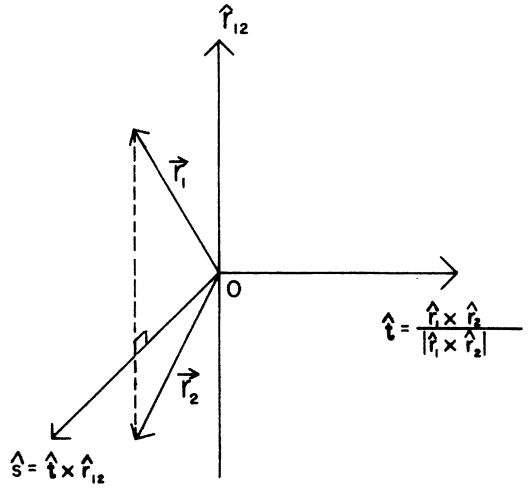

FIG. 1. The two-electron body frame. The set $(\hat{\mathbf{s}},\hat{\mathbf{t}},\hat{\mathbf{r}}_{12})$ forms a right-handed system. The two electrons are on the $\hat{\mathbf{s}}-\hat{\mathbf{r}}_{12}$ plane.

Hence

$$\tan[\chi(\alpha,\theta_{12})]=\sin\theta_{12}/(\cot\alpha-\cos\theta_{12}) . \tag{9}$$

We next demonstrate the decomposition of a wave function into partial components assuming that it is explicitly known in the laboratory coordinates. Suppose

$$\psi(\mathbf{r}_1,\mathbf{r}_2)=\sum_{l_1,l_2}\psi^L_{l_1l_2}(r_1,r_2)\mathcal{Y}_{l_1l_2LM}(\hat{\mathbf{r}}_1,\hat{\mathbf{r}}_2) . \tag{10}$$

Substituting Eq. (4) into (10) we get

$$\psi(\mathbf{r}_1,\mathbf{r}_2)=\sum_{Q}\psi^L_Q(R,\alpha,\theta_{12})D^{(L)}_{QM}(\hat{\Omega}) , \tag{11}$$

where

$$\psi^L_Q(R,\alpha,\theta_{12})=\sum_{l_1,l_2}\psi^L_{l_1l_2}(R\cos\alpha,R\sin\alpha) \times\mathcal{Y}_{l_1l_2LQ}(\hat{\mathbf{r}}'_1,\hat{\mathbf{r}}'_2) \tag{12}$$

and $-L\le Q\le L$.

Let us consider the symmetry under particle exchange (see Appendix A). In the body frame, particle exchange is equivalent to the replacement $\alpha\to\pi/2-\alpha$ from which

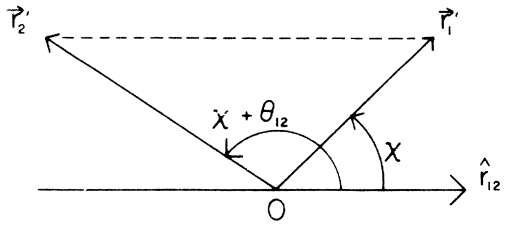

FIG. 2. Geometrical meaning of $\chi(\alpha,\theta_{12})$.

$\chi\to\pi-(\chi+\theta_{12})$. Using a property of the associated Legendre function, we get

$$\psi^L_Q(R,\pi/2-\alpha,\theta_{12})=\pi(-1)^{S+Q}\psi^L_Q(R,\alpha,\theta_{12}) , \tag{13}$$

where S is the total spin, and the symbol π on the right is $+1$ and -1 for even and odd parity states, respectively. We shall use a shorthand notation for this phase factor:

$$A=\pi(-1)^{S+T} , \tag{14}$$

where $T=|Q|$. The index A [Ref. 7(d)] determines the reflection symmetry of the radial wave function with respect to the $\alpha=\pi/4$ axis. Thus A serves as an index of radial correlation. In the body frame, we also have

$$\mathcal{Y}_{l_1l_2L-Q}(\hat{\mathbf{r}}'_1,\hat{\mathbf{r}}'_2)=\eta(-1)^Q\mathcal{Y}_{l_1l_2LQ}(\hat{\mathbf{r}}'_1,\hat{\mathbf{r}}'_2) \tag{15}$$

with $\eta=\pi(-1)^L$. Therefore we define for $Q\neq0$

$$\tilde{D}^{(L)}_{TM}(\hat{\Omega})=\frac{1}{\sqrt{2}}[D^{(L)}_{|Q|M}(\hat{\Omega})+\eta(-1)^TD^{(L)}_{-|Q|M}(\hat{\Omega})] , \tag{16}$$

which is equivalent to the usual molecular rotor function. Equations (15) and (16) are familiar in molecular physics and serve as a geometrical interpretation of Eqs. (3.16)–(3.17) of Herrick, Kellman, and Poliok[2] (to be referred to as HKP hereafter).

Another symmetry property which proves useful later is the replacement of $\theta_{12}\to2\pi-\theta_{12}$, that is, the reflection symmetry with respect to the $\theta_{12}=\pi$ axis. This replacement is equivalent to $\chi\to-\chi,\chi+\theta_{12}\to2\pi-(\chi+\theta_{12})$. Thus, it follows readily that

$$\psi^L_Q(R,\alpha,2\pi-\theta_{12})=(-1)^T\psi^L_Q(R,\alpha,\theta_{12}) , \tag{17}$$

which provides the relation between the parity of the bending vibration and the rotational quantum number T.

III. HYPERSPHERICAL CHANNEL FUNCTIONS IN THE BODY FRAME

We examine the details of radial and angular correlations by exploiting our decomposition procedure. This procedure applies to wave functions calculated in any scheme such as the configuration-interaction method, close-coupling method etc. Here some hyperspherical channel functions of He below the He^+ ($N=3$) limit are analyzed. First in Sec. III A we review the essentials of the hyperspherical method. The hyperspherical wave functions are then decomposed into rotational components. In Sec. III B the purity of each rotational state is examined as it serves as a measure of the effectiveness of Lin's classification scheme. In Sec. III C we discuss the bending vibrational mode and associated quantum numbers. Finally, the analogy between the radial correlation quantum number A and the stretching modes of triatomic molecules is discussed in Sec. III D.

A. The hyperspherical method (Refs. 7–10)

In the hyperspherical method, the character of doubly excited states is unraveled by examining the two-electron wave functions in hyperspherical coordinates. Using a

quasiseparable approximation, the two-electron wave functions are expressed as

$$\psi^i_\mu(R,\Omega)=F^i_\mu(R)\phi_\mu(R;\Omega)\ , \tag{18}$$

where ϕ_μ is the hyperspherical channel function and $F^i_\mu(R)$ is the ith hyperradial wave function in channel μ. We use Ω to denote collectively the hyperangle α and the spherical angles of the two electrons. The channel function is obtained by solving the two-electron Schrödinger equation under the constraint that the electrons move on the hyperspherical shell defined by

$$R=(r_1^2+r_2^2)^{1/2}=\text{const}\ , \tag{19}$$

i.e., by requiring that it satisfies the eigenvalue equation

$$H_{R=\text{const}}\phi_\mu=U_\mu(R)\phi_\mu\ . \tag{20}$$

The eigenvalues $U_\mu(R)$ play a role analogous to that of molecular potential curves and can be used for approximate determination of resonance positions.[7-10]

Throughout our work, channels are labeled in accordance with Lin's prescription,[7(d)] namely, by $(K,T)^A_N{}^{2S+1}L^\pi$. The index K originates from the two-electron Stark basis introduced by Herrick[16] and is related to the bending-vibrational quantum number. We shall return to this discussion shortly. T and A are defined by Eq. (14); N is the principal quantum number of the electron in He^+; the rest are well-known quantum numbers. We supplement this label by introducing an index $\eta=\pi(-1)^L$ in front of T, that is, when $\eta<0$ we write $(K,-T)^A_N{}^{2S+1}L^\pi$, as done by others.[5] Since the possible atomic configurations with a given L depend on the parity, this separates two groups of atomic configurations. This labeling makes sense only if the quantum numbers K and T as well as the atomic shell N are unambiguously defined.

In the present work, we determined the channel functions variationally using the analytic basis functions of Lin[7] complemented by hyperspherical harmonics. A typical channel function has the form

$$\phi_\mu(R;\alpha,\hat{\mathbf{r}}_1,\hat{\mathbf{r}}_2)=\sum_{l_1,l_2} g^\mu_{l_1l_2}(R;\alpha)\mathscr{Y}_{l_1l_2LM}(\hat{\mathbf{r}}_1,\hat{\mathbf{r}}_2)\ . \tag{21}$$

Radial functions $\{g^\mu_{l_1l_2}(R;\alpha)\}$ are used as the input to $\psi^L_{l_1l_2}(\hat{\mathbf{r}}_1,\hat{\mathbf{r}}_2)$ of Eq. (12).

B. Purity of rotational states

The symbol A, as defined in (14), has a close connection with the value of T. According to the decomposition (11), if there is only one single rotational component T, then the radial correlation quantum number A will be either $+$ or $-$. Thus the purity of radial correlation quantum number A is related to the purity of rotational states. To examine the purity of quantum numbers T and A in the labeling of channels, we display the density plots of rotational components for hyperspherical channel functions.

As an illustration of the purity of rotational states, we display in Fig. 3 the density plots of the $(1,1)^-_3{}^3P^o$ and $(1,1)^+_3{}^1P^o$ channel functions of He at the values of R where their respective potential curves bottom out. The

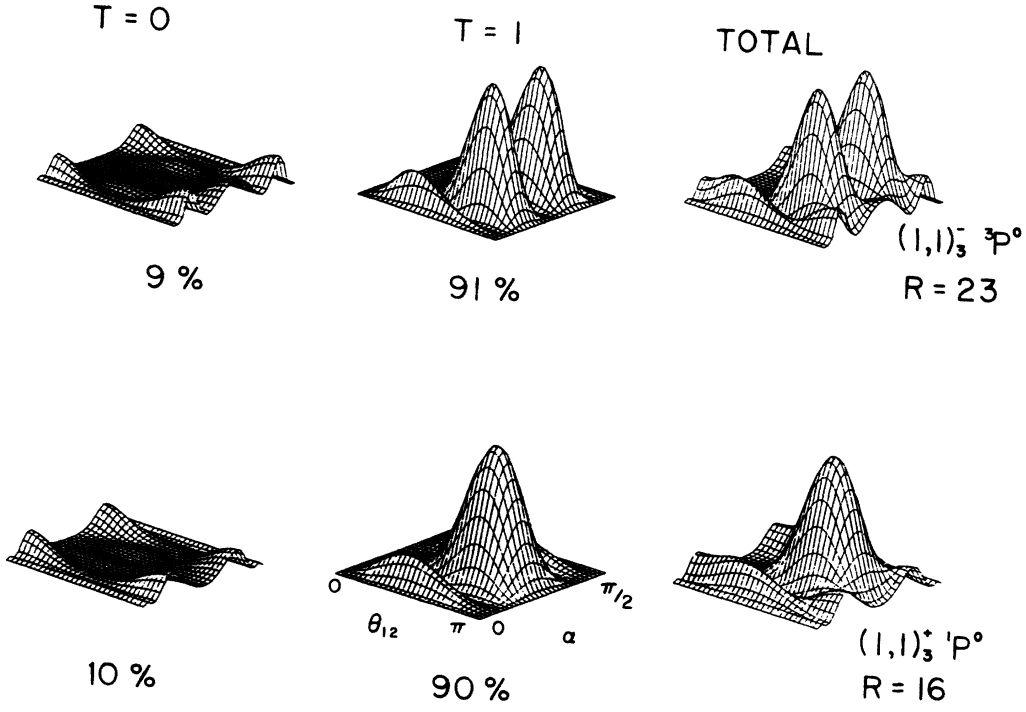

FIG. 3. Density plots of the $(1,1)^+_3{}^1P^o$ and $(1,1)^-_3{}^3P^o$ channels. Percentage represents the contribution to the normalization from each T component. The axes for all the plots are identical. Their labels are shown in the middle figure of the second row.

percentage indicated represents the contribution to the normalization constant from each T component, the partial normalization constant being defined by

$$N_T(R)=\frac{1}{8\pi^2}\int d\alpha\, d(\cos\theta_{12})\,|\psi_T|^2 . \tag{22}$$

Each channel function is normalized so that the normalization coefficients from all the rotational components adds up to unity. For $^3P^o$, the $T=1$ component has 91% of the integrated density. According to (14), $A=-$ for this component and the function must vanish along $\alpha=\pi/4$. The density plot for the $T=1$ component clearly exhibits this property. This channel also has a 9% contribution from the $T=0$ component. The density plot for the $T=0$ component has an antinode at $\theta_{12}=\pi$ and at $\alpha=\pi/4$, is consistent with Eqs. (14) and (17). The fact that the dominant component of this channel is labeled by $T=1$, $A=-$ is in fact consistent with Lin's label, $(1,1)^-$, for this channel. Similarly, for $^1P^o$ the $T=1$ component represents a 90% contribution and the $T=0$ a 10% contribution at $R=16$. In this case, the $T=1$ component has $A=+$ and a node at $\theta_{12}=\pi$, while the $T=0$ component has $A=-$ and an antinode at $\theta_{12}=\pi$. The fact that $T=1$ is the dominant component is consistent with the designation of $T=1$ and $A=+$ for this channel.

Within a given N manifold, the purity of rotational states decreases for the more highly excited channels. To illustrate this, we show in Fig. 4 the density plots of the five $^1D^e$ ($N=3$) channels of He at their respective potential minima. Notice that the normalization constants for

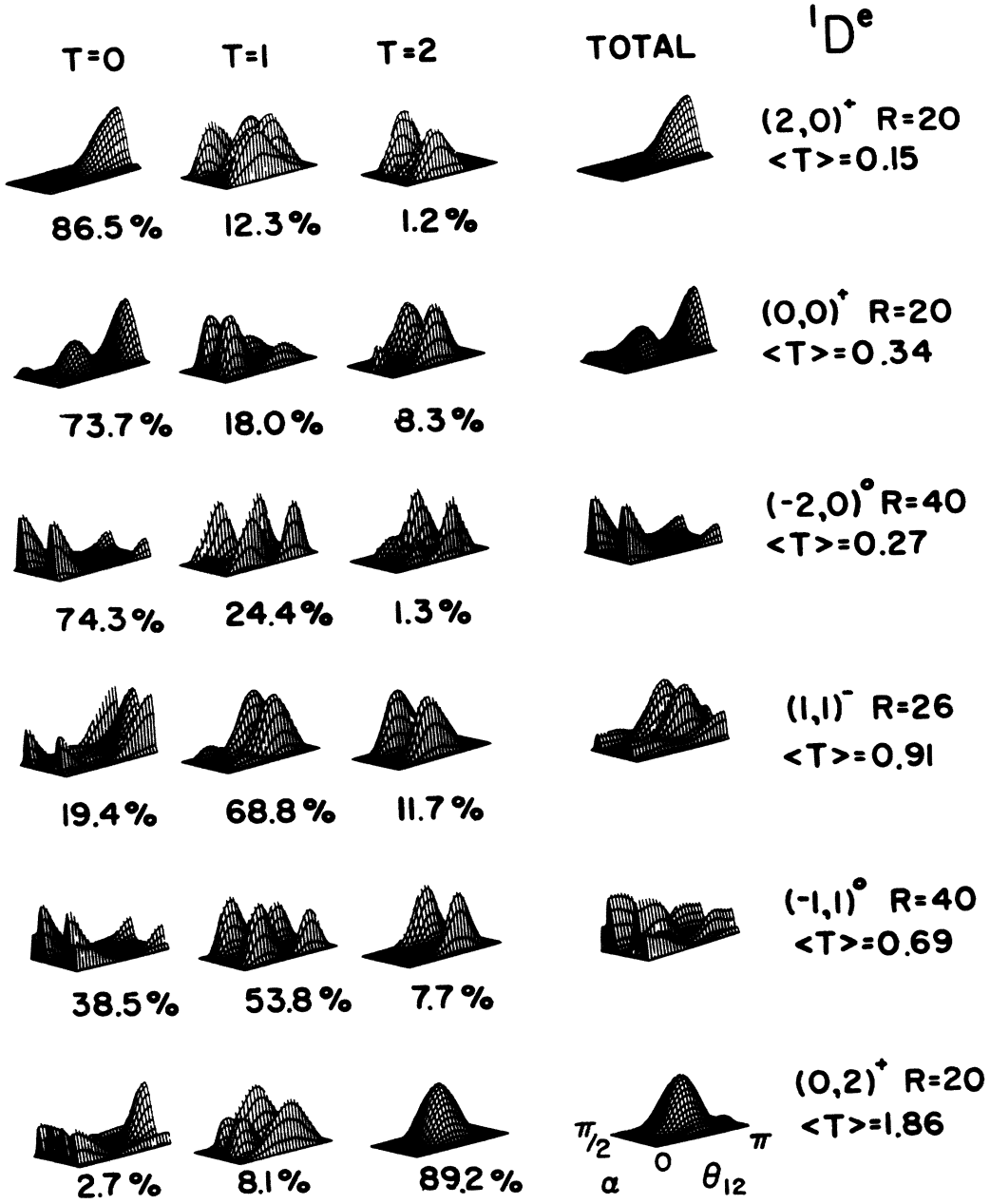

FIG. 4. Density plots of the He ($N=3,{}^1D^e$). Channels are at the position of their potential minima. $\langle T\rangle$ is the average value of T. The axes for all the plots are identical to the ones shown at the right lower corner.

different rotational components become more smoothly distributed for the higher channels. The quantum numbers T and A for these channels are less well defined. We also note that the relation between the dominant T component and A is indeed consistent with Eq. (14) for the lower channels for which $A=+$ or $-$ but not 0.

The purity of rotational states optimizes roughly in the range where the potentials bottom out. This is the region that the lowest resonant state of each channel occupies in each well. To illustrate how the purity of the rotational state depends on R for each channel, we show in Fig. 5 the contribution to normalization from each $T=1$ component of the five $^1P^o$ ($N=3$) channels and from each $T=0$ and $T=1$ component of the six $^1D^e$ ($N=3$) channels of He. The dashed lines represent the interpolated region where the potential curves exhibit rather sharply avoided crossings. We note that the low-lying channels show greater purity of rotational states while the higher channels tend to violate the purity of T more severely. Moreover, we notice that the rotational quantum number T is ill respected at large values of R. This aspect is understood by examining the large-R limit of $H_{R=\text{const}}$,

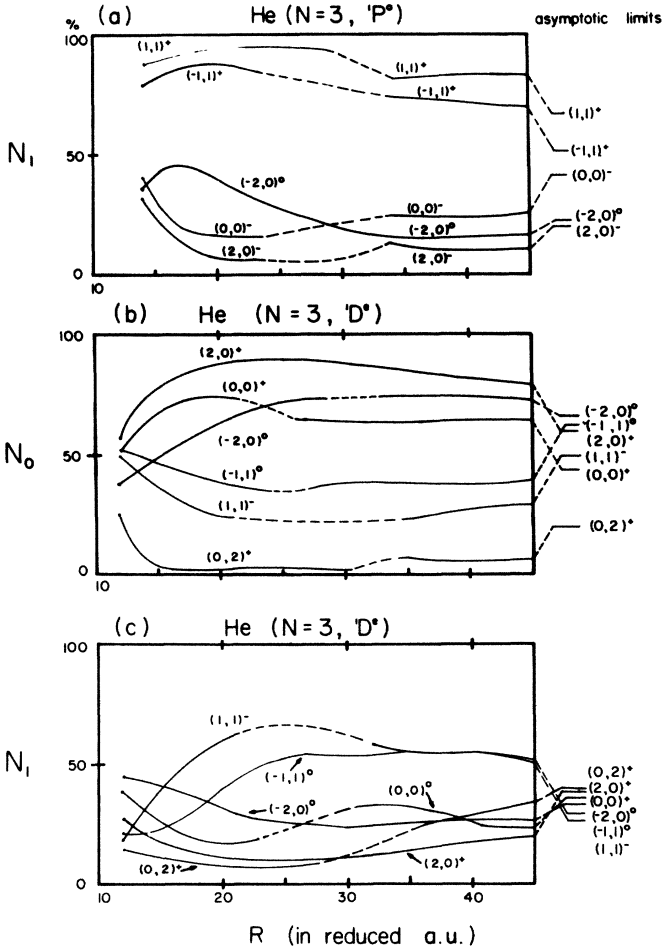

FIG. 5. Normalization coefficients $N_T(R)$, Eq. (22), as a function of R for the He ($N=3$,$^1P^o$,$^1D^e$) channels of Figs. 3 and 4; (a) shows N_1 of the $^1P^o$ channels, (b) and (c) show N_0 and N_1 of the $^1D^e$ channels, respectively. The asymptotic limits of N_T corresponding to $R\to\infty$ for each channel are indicated on the right.

$$H_{R=\text{const}}\simeq\left[-\frac{1}{2}\frac{d^2}{dr_2^2}+\frac{l_2^2}{2r_2^2}-\frac{Z}{r_2}\right]-\frac{Z-1}{R}$$

$$+\frac{l_1^2+2\hat{\mathbf{r}}_1\cdot\hat{\mathbf{r}}_2}{2R^2}+O(1/R^3)\,, \tag{23}$$

and $r_1\simeq R\gg r_2$. (Minor subleties due to the difference between R and r_1 are ignored here. The reader who seeks rigor should refer to the Appendix of Ref. 8.) The terms in the large parentheses represent the Coulomb Hamiltonian, and the rest the perturbation by the outer electron which acts as the source of an external electric field. The field direction is along $\hat{\mathbf{r}}_1$ which in this limit coincides with $\hat{\mathbf{r}}_{12}$ to order r_2/r_1. The term $l_1^2/2R^2$ describes the angular motion of the outer electron, indicating that the electric field is not along a fixed direction. The effect of this term is to dilute the purity of rotational states as seen above.

C. Vibrational quantum numbers

Zero-order vibrational states do not emerge automatically in our body-frame analysis since they belong to the internal vibration of the pair's orbits. Earlier numerical studies by Lin[7c] indicate that the expectation value of the angle θ_{12} is fairly constant over a wide range of R for each adiabatic channel, that is, the angle of relative orientation is quantized and is an approximate adiabatic invariant. We exploit this fact in order to see the approximate quantization of the vibrational mode and to associate it with the vibrational energy.

If we neglect the angular motion of the outer electron in Eq. (23), the problem becomes identical to the Stark problem of the hydrogenlike atom where the electric field is along the r_1 axis. Diagonalization of the Hamiltonian (23) can be readily accomplished to first order using an $O(4)\times O(4)$ reduction scheme of Herrick for each value of the total angular momentum L. This leads to the eigenvalues

$$H_{R=\text{const}}\simeq-\frac{Z^2}{2N^2}-\frac{Z-1}{R}-\frac{3NK}{2Z}\frac{1}{R^2}$$

$$+[l_1^2/2R^2+O(1/R^3)],\quad R\gg r_2 \tag{24}$$

where K takes integral values $N-1-T\geq K\geq -N+1+T$. This number K relates to the number of nodes n in θ_{12} by

$$n=N-1-K \tag{25}$$

in the present limit and approximation. In effect, the quantum number K is a measure of the polarizability. We now consider the adiabatic continuation of this quantum number K all the way into the strongly correlated region, where R is of the order of N^2/Z. To this end, we defined the effective measure of the dipole polarizability $K_{\text{eff}}(R)$ as $K_{\text{eff}}(R)=(2Z/3N)R^2V_{\text{dip}}$ where V_{dip} is the dipole interaction term

$$V_{\rm dip}(R,\alpha,\theta_{12})=\begin{cases}\dfrac{1}{R^2}\dfrac{R\sin\alpha}{\cos^2\alpha}\cos\theta_{12}, & 0\le\alpha\le\pi/4\\ \dfrac{1}{R^2}\dfrac{R\cos\alpha}{\sin^2\alpha}\cos\theta_{12}, & \pi/4\le\alpha\le\pi/2\ .\end{cases} \tag{26}$$

The near constancy of the expectation value of θ_{12} suggests the near constancy of $K_{\rm eff}(R)$. Some examples are shown in Fig. 6 for the He ($N=3$, $^1P^o$,$^1D^e$) channels. We notice that $K_{\rm eff}(R)$ is slowly dependent on R and is close to the integer K used to label the channels. This feature is particularly well respected by + and − type channels but not so well by 0 channels. In some cases, however, noticeable departures from the nearest integer take place. At moderate values of R, higher multipole terms become increasingly important as they represent the nonuniformity of the electric field one electron exerts on the other. Nevertheless, the nodal structure of the wave function does not differ drastically from that at large R due to the quasi-invariance of θ_{12} or of $K_{\rm eff}(R)$.

The observed trend suggests an empirical formula for the local spring constant

$$\nu(R)=\frac{3N}{2ZR^2}\ . \tag{27}$$

The potential curves for channels with the same L, T, and A are then displaced by an amount proportional to $\nu(R)$ at each R. For resonant states with equal effective size $R_{\rm eff}$, the vibrational energy spacing should be given by

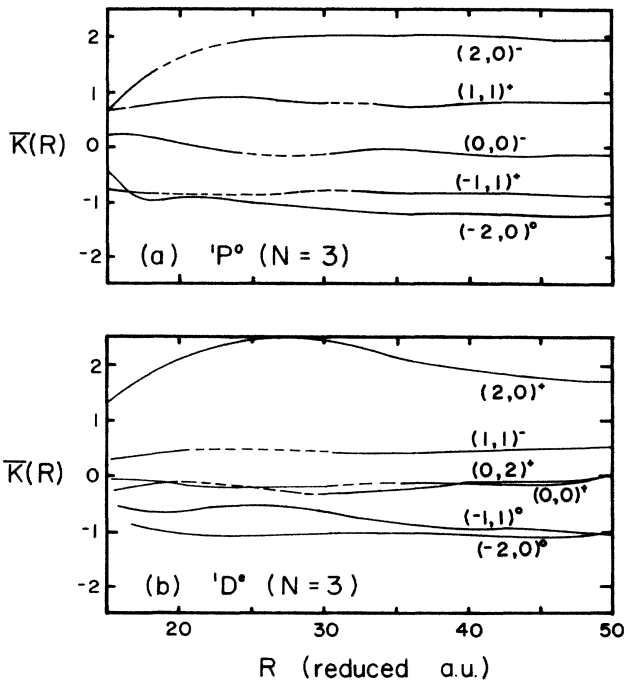

FIG. 6. R dependence of $\bar{K}(R)=(2Z/3N)R^2V_{\rm dip}$ for each channel of (a) the $^1P^o$ ($N=3$) manifold and (b) the $^1D^e$ ($N=3$) manifold of He. Dashed lines are used to indicate the region where diabatic crossing has been imposed.

$$\Delta E=\nu(R_{\rm eff})\Delta K\ . \tag{28}$$

In molecular physics, it is customary to use the vibrational quantum number v which is related to the vibrational energy spacing $\nu(R_{\rm eff})$ by

$$E_v=\nu(R_{\rm eff})(v+1)\ , \tag{29}$$

where the number 1 stems from the sum of the zero-point energies of two identical vibrators. An alternative labeling of the channel by v is possible by interpreting K as

$$K=N-v-1\ , \tag{30}$$

thereby v ranges over non-negative integers starting from T. The number of nodes n in θ_{12} provides a measure of the angular degree of excitation. The relation between n and v is

$$n=(v-T)/2\ , \tag{31}$$

where n takes integral values (n coincides with one of the Stark quantum numbers of the hydrogenlike atom in the limit of large R). Though there are other quantum numbers equivalent to K, v, or n, we shall not delve into them because we use only these in this present paper.

D. Radial correlation and molecular stretching modes

In Sec. III B we demonstrated through specific examples how the nodal structure of a channel function near $\alpha=\pi/4$ is related to the rotational quantum number T. The label A is thus nothing but the parity of the channel function under the reflection with respect to the line given by $\alpha=\pi/4$. It is worthwhile to make a connection with the molecular stretching modes.

Near $\alpha=\pi/4$, we may use $\xi=\pi/4-\alpha$ to represent the displacement along α. We recognize the correspondence

$$\begin{aligned}s&=r_1+r_2\simeq\sqrt{2}R\ ,\\ u&=r_1-r_2\simeq\sqrt{2}R\xi\ ,\end{aligned} \tag{32}$$

where s stands for the symmetric stretch and u for the antisymmetric stretch. Near $\alpha=0$, however,

$$\begin{aligned}r_1&\simeq R\ ,\\ r_2&\simeq R\alpha\ .\end{aligned} \tag{33}$$

In molecular physics,[17–19] r_1 and r_2 are referred to as the local stretch mode; r_2 in particular describes the harmonic oscillation of a pair of atoms in the Morse-type potential. Their roles are interchanged near $\alpha=\pi/2$. This smooth evolution of R and α from the region of molecular complex to that of decoupled local modes is extremely useful because the general motion of particles involves a coupling of molecular modes and local modes.

The +, −, classification scheme utilizes the degree of excitation in the antisymmetric stretch mode u, Eq. (32). Successive levels in the same + potential curves are all even states in the u mode whereas levels in the − curves are odd states. Levels in each potential well are distinguished by the number of nodes in R which changes it principal character from the symmetric stretching mode to the local stretching mode as the system's size increases. The intrashell states thus exhibit the molecule modes most

strongly owing to their large concentration in the region near $\alpha=\pi/4$ where the complementary nature of α and R becomes notable.

We would like to direct the reader's attention to the reduced probability densities displayed in Figs. 1(b), 2(a), and 3 of Ref. 7(a) and Figs. 6 or Ref. 19(a) in order to substantiate the present discussion. The comparison is useful for seeing the connection between formally different problems. The former represent a series of doubly excited states of He whereas the latter represent a series of resonances in coupled harmonic oscillators which model eigenstates of a triatomic molecule. The symmetric stretch mode in both examples is seen to form astride the potential ridge where the local kinetic energy has a minimum or a saddle point.[20] The reader can find the display of an even-odd doublet in Figs. 1(e) and 1(f) of Ref. 19(a) which is analogous to our Fig. 3 demonstrating a + and − doublet. The coupling of the symmetric stretch with the local modes and the antisymmetric stretch are important for understanding the excitation probability, decay rate,[9,19,20,21] etc. However, this subject is beyond the scope of the present paper.

Before closing this section it is appropriate to comment on channels which do not exhibit radial stretching modes, namely the channels labeled $A=0$. In these channels the overlap between the inner and outer electrons is hardly substantial for forming moleculelike normal modes since the electrons are localized in potential valleys near $\alpha=0$ or $\pi/2$ or to put it differently, the dynamical tunneling[19(a)] from one valley to another is extremely weak. Instead they have been shown to exhibit behavior anticipated by the independent-particle model.

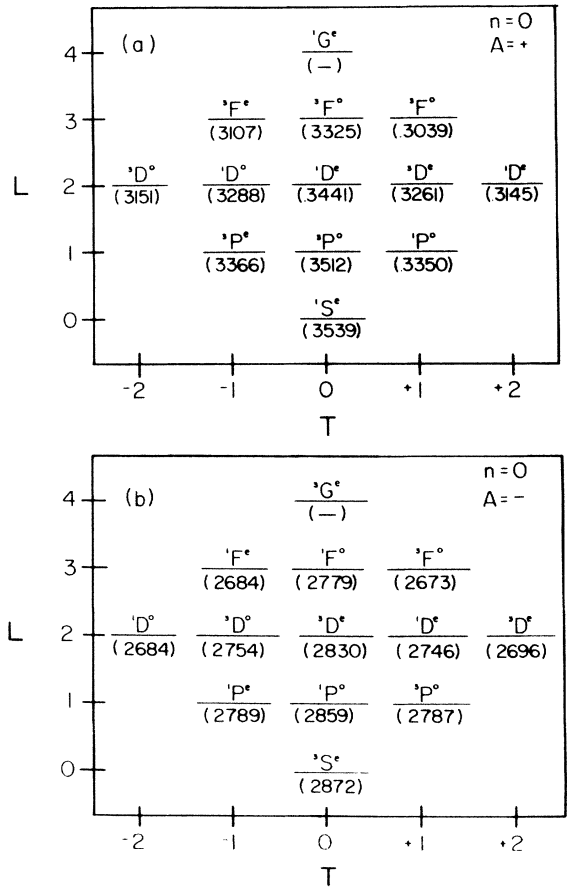

FIG. 7. (a) $N=3$ intrashell levels of He in the d-supermultiplet scheme, (b) the lowest state in each channel of He ($N=3$) in the d-supermultiplet scheme. Levels are given in parentheses in atomic units. Data from Ref. 22.

IV. A UNIFIED VIEW OF MOLECULELIKE MODES

We have seen thus far how the qualitative moleculelike picture of two-electron correlations fits into the framework of the hyperspherical method. Accordingly, it is adequate to classify radial correlation by the even or odd parity of the antisymmetric stretch indicated by A, angular excitation labeled by K and T, and exploit supermultiplet schemes to discern the systematics of relative energy levels. The classification scheme thus relies on the fact that clear-cut manifestation of the moleculelike modes respect the hierarchical order in the magnitude of correlation energies, namely, $U_{\pm}>U_v>U_r$ where $U_{\pm},\ldots$ are the separation of the + and − doublet curves and the local vibrational and rotational energies, respectively. The higher angular excitation leads to the less clear-cut order in correlation energies and to the sometimes noticeable admixture of other modes.

When the molecular picture applies, the radial correlation divides moleculelike modes into $A=+$ and $A=-$ groups. In each group, states are classified by their angular-correlation patterns. There are two well-defined schemes. One is the d-supermultiplet scheme which utilizes the number of nodes in θ_{12}, namely, n discussed in Sec. III C to regroup energies. An example is shown in Fig. 7 for the lowest $n=0$ states: (a) for $A=+$ subgroup and (b) for the $A=-$ subgroup for doubly excited states of He ($N=3$). The vertical axis corresponds to L and the horizontal axis is labeled by $(K,\pm T)$. Since n is fixed, K and T are constrained by Eq. (25). The numbers in brackets are energy levels in a.u. Note that there is an unambiguous correspondence between the + type and − type supermultiplets, namely, the interchange of the spin labels $1\leftrightarrow 3$. This is simply because the antisymmetry of the radial wave function induced by the radial excitation must be compensated for by the change in symmetry of the spin function [see Eq. (14)]. The η parity is unaffected by this operation and retains the usual convention of the supermultiplet scheme. Another scheme is known as the I supermultiplets which puts more emphasis on the rotational degree of freedom. A new label $I=L-T$ $(0<I<2N-2)$ is introduced to classify angular modes. Since the component of the total angular momentum orthogonal to $(\mathbf{L}\cdot\hat{\mathbf{r}}_{12})\hat{\mathbf{r}}_{12}$ is $\mathbf{N}=\mathbf{L}-(\mathbf{L}\cdot\hat{\mathbf{r}}_{12})\hat{\mathbf{r}}_{12}$ and $\mathbf{N}^2=\mathbf{L}^2-T^2$ (as in molecules), we have in the classical limit $N^2=(L+T)(L-T)$. So the number I pertains, loosely speaking, to the rotational degree of freedom orthogonal to that represented by T. With K as the vertical axis and $\pm T$ as the horizontal axis, a diamond similar to Fig. 7 can be constructed for each I[2]

The moleculelike normal modes motivated HKP to fit intrashell energy levels to the molecular-term formula. Three aspects peculiar to atoms were addressed. First is that the rotational constant evaluated using the probable gyro radius (=hyperradius R), namely,

$$B=\tfrac{1}{2}\overline{R}^{\,2}\,, \tag{34}$$

implied that the probable hyperradius would be unrealistically bigger than the size of the atom. Second, the probable hyperradius appears to shrink as the system increases rotational energy, that is, the centrifugal distortion corresponds to the contraction of the atom. Third, the quasidegenerate T doublets showed a tendency for the states with $\eta=+$ to be somewhat higher than those with $\eta=-$. For the latter two, there are already heuristic arguments explaining the tendencies. There is nevertheless a question. For example, do they also hold for the $-$ type supermultiplets. We examine these phenomena in the rest of this section.

As a preliminary, we give here a result of fitting the calculated energy levels of Lipsky *et al.*[22] to the molecular-term formula[1(a)]

$$\begin{aligned}E=&E_N+\nu(v+1)+X(v+1)^2\\&+GT^2+[B-\alpha(v+1)][L(L+1)-T^2]\\&-D[L(L+1)-T^2]\,.\end{aligned} \tag{35}$$

Their calculated energy levels are given in parentheses in Fig. 7. Applying Eq. (4.12) of HKP, we arrive at Table I. The values of $\overline{R}$ calculated from Eq. (34) are $\overline{R}=28$ and 39 a.u. for the $+$ and $-$ supermultiplets, respectively. These are indeed gross overestimates in view of the He potential curves for $N=3$. (Note that the hyperradius R shown in Fig. 8 is given in reduced units, i.e., ordinary atomic units multiplied by Z.) The negativity of D implies the contraction of the system with increasing L. We see D is also negative for the $-$ multiplets. The comparison of T doublets show that with the exception of $^1D^o$ and $^3D^e$ the $\eta=+$ states are higher than the corresponding $\eta=-$ states. (This exception may be merely due to numerical inaccuracy in the calculation of Ref. 22.)

TABLE I. Molecular term constants obtained by fitting the lowest $+$ and $-$ states of He** ($N=3$) to the molecular-term formula, Eq. (35). Data taken from Ref. 22. Numbers in square brackets represent powers of ten, e.g., $1[-2]=1\times10^{-2}$.

	+	−
E	0.3695	0.2943
ν	1.45[−2]	6.57[−3]
X	1.17[−3]	4.90[−4]
G	−1.05[−3]	−5.21[−4]
B	6.46[−4]	3.23[−4]
α	−5.97[−4]	−3.21[−4]
D	−6.49[−5]	−1.04[−5]

A. The origin of the rotational constant B

We must begin this section with a word of warning. The molecular-term formula (35) attempts to attribute the higher-order corrections to the anharmonicity of the bending vibration potential, centrifugal distortion, etc. In atoms, the impurity of the (K,T) states is an equally important contributor to the departure from the lowest-order formula,

$$E(L,v,T)=E_N+\nu(v+1)+B[L(L+1)-T^2]+GT^2\,. \tag{36}$$

To avoid overweighing high-lying states, let us employ a few lowest states to fit Eq. (36). Thus, in particular,

$$\begin{aligned}\Delta E=&E(L',v,T)-E(L,v,T)\\=&(L'+L+1)(L'-L)B\,.\end{aligned} \tag{37}$$

Applying this to $(2,0)_3^+\,{}^1S^e,\,{}^3P^o,{}^1D^e$ we obtain Table II(a). The estimate of $\overline{R}$ is still larger than the average value of R expected from Fig. 8. The contraction of the system is undeniable, however. A similar trend holds with the $-$ counterparts $(2,0)_3^-\,{}^3S^e,\,{}^1P^o,{}^3D^e$ as in Table II(b), though the trend is weaker.

The departure of $\overline{R}$ from the expected value of R in Fig. 8 is not surprising in view of the following fact. In atoms, the rotational constant does not simply arise from kinematics. Here we are concerned with the effective rotation of the electrons' orbits. We must thus identify the inertia of the orbits, namely that part of the two-electron Hamiltonian which contributes dominantly to the rotor energy. To do so we first consider the limit of high Z in which case the bielectronic interaction is perturbative. One of the SO(4) bases $|PQLM\rangle$ [Eq. (3.15) of HKP] is a good one for perturbation calculation where $P=2N-1-(v+1)$. An approximate result has been obtained by HKP exploiting the series expansion in $\mathbf{r}_1\cdot\mathbf{r}_2/R^2$ to the leading order,[1(a)] and is given by

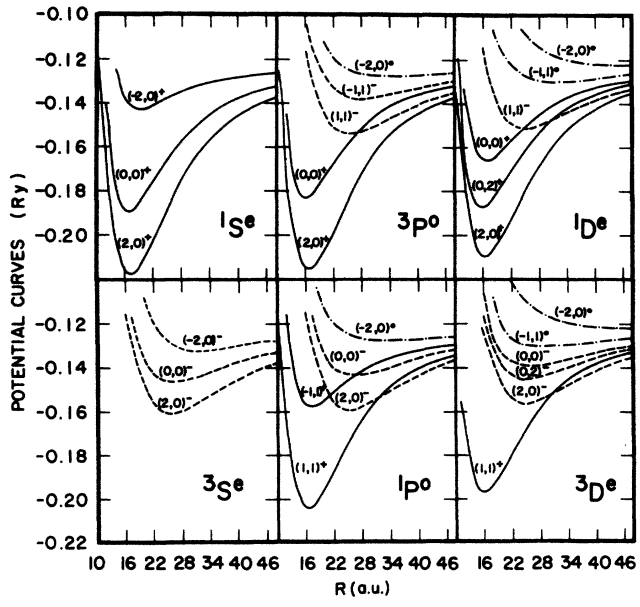

FIG. 8. Reproduction of He ($N=3$) potential curves from Ref. 7(d). R in *reduced* a.u., U_μ in *reduced* Ry.

TABLE II. Estimate of B and $\bar{R}$ [see Eq. (34)] from the lower members of the rotational series for a given v and T. [See Eq. (37).] (a) $A=+$, (b) $A=-$. Numbers in square brackets represent powers of ten, e.g., $1[-2]=1\times10^{-2}$.

$L-L'$	$S-P$	$S-D$	$P-D$
	(a)		
B	1.37[−3]	1.63[−3]	1.76[−3]
$\bar{R}$	19	18	17
	(b)		
B	6.60[−4]	7.11[−4]	7.30[−4]
$\bar{R}$	27.5	26.5	26.2

$$\left\langle PQLM\left|\frac{1}{r_{12}}\right|PQLM\right\rangle$$
$$\simeq(4Z/N)(24N^2+24+14\mathbf{B}^2+2\mathbf{L}^2)^{-1/2}$$
$$\simeq\frac{Z}{\sqrt{5}N^2}\left[1+\frac{1}{80N^2}[6(\mathbf{L}^2-\mathbf{T}^2)-\mathbf{T}^2+28N(v+1)\right.$$
$$\left.-7(v+1)^2+7]+O(1/N^3)\right]. \quad (38)$$

We identify then

$$B\simeq\frac{3}{40\sqrt{5}}\frac{Z}{N^4}. \quad (39)$$

The rotational constants obtained by Eq. (39) for the $N=3$ rotor series of He, Li^+, Be^{2+} and B^{3+} are about a factor of 2 smaller than the values deduced from Ref. 22. Since the radial correlation which tends to contract the system by mutual screening and other effects are not included, one should not take this discrepancy too seriously. Equation (39) is a rough approximation which attributes the origin of the rotational constant to the bielectronic repulsion. This approximation leads to the linear dependence of B on Z which trend is well respected by the values of B deduced from the energy levels in Ref. 22, see Table III. In summary, this behavior of the rotational constant B contrasts with that of molecules. The rotation of molecules can be treated as quasirigid rotors because the positions of the atoms are localized and are determined by the electronic potential surface, where the atoms perform simple harmonic-type oscillation about the potential minima. Electrons in a doubly excited atom perform periodic motion about the nucleus; it is the effective rotation of their orbits which contributes to the rotational energy.

The linear dependence of B on Z arose from that of $1/r_{12}$ on Z. The same linear law holds with the vibrational constant $\nu(\bar{R})$, Eq. (27). This is checked in Table IV to complete our examination of the main molecular constants. An estimate of ν from Eq. (38) is $\nu=(7Z/20\sqrt{5})N^{-3}$. For He this gives 0.012 a.u. which is to be compared with the value 0.0145 a.u. given in Table I. Note also the ratio $\nu/B\simeq14N/3$ from Eq. (38) is close to the empirical rule $\nu/B\simeq4N$ (HKP).

B. The rotational contraction of intrashell states

Evidence of the rotational contraction, namely, the negativity of D of Eq. (35), was noticed by HKP not only by the energy fitting but also from the fact that the position of the hyperspherical minimum moves inward as L increases (see Fig. 8). (This trend does not hold for $A=0$ channels.) Using the $|PQLM\rangle$ basis of HKP again, one can evaluate $\langle PQLM|R^2|PQLM\rangle$. The result is

$$R^2\simeq\frac{N^2}{8Z^2}[40N^2+17-6\mathbf{L}^2+3T^2-12N(v+1)$$
$$+3(v+1)^2] \quad (40)$$

[Eqs. (A7) and (8) of HKP used]. The negative coefficient of $\mathbf{L}^2$ indicates the rotational contraction. Let us look into this effect more closely. In Fig. 9 we show the sectional view of the reduced density as a function of α. The value of θ_{12} is set to where the density is maximum. Figure 9(a) is for $(2,0)_3^+$ and Fig. 9(b) is for $(1,1)_3^+$ channels, respectively, the latter having higher angular correlation energy. In both cases the α wave function moves toward $\alpha=0$ and peak less at $\alpha=\pi/4$ with increasing L. In the configuration-interaction language, this is because the larger L is, the more weight is placed on orbital (Nl_1,nl_2) of larger l_1 and l_2, or in classical terms, on orbits of smaller eccentricity, hence the average size $r=\langle R\sin\alpha\rangle$ tends to be smaller. (Note $\langle r^2\rangle=\langle R^2\rangle/2$.) Because of this reduction in the amplitude near $\alpha=\pi/4$, the corresponding sectional view in θ_{12} (Fig. 10) shows that the charge density shifts toward small θ_{12} as L increases. This is in contrast with the prediction of the rigid-bender model where the shift is toward $\theta_{12}=\pi$ as L increases. This can also be seen from the O(4) expectation value of $\cos\theta_{12}$ given by Eq. (3.31) of HKP, namely,

$$\langle\cos\theta_{12}\rangle=-[8N^2+1+12N(v+1)$$
$$+3(v+1)^2-2\mathbf{L}^2]/8N^2. \quad (41)$$

The negative coefficient of $\mathbf{L}^2$ implies that $\langle\theta_{12}\rangle$ decreases from π as L increases. In other words, in doubly excited states with large L, both the radial and angular correlations are weakened.

TABLE III. Z scaling of the rotational constant B. Formula (39) predicts that B/Z is a constant. [B was calculated using the energy spacing between ${}_3(2,0)_3^+\ {}^1S^e$ and ${}^3P^o$.] Numbers in square brackets represent powers of ten, e.g., $1[-2]=1\times10^{-2}$.

Z	2	3	4	5
B	1.36[−3]	2.24[−3]	3.09[−3]	3.95[−3]
B/Z	0.68[−3]	0.75[−3]	0.77[−3]	0.79[−3]

TABLE IV. Z scaling of the vibrational constant ν. Formula (27) predicts that ν/Z is a constant. [ν was calculated using the energy spacing between ${}_3(2,0)_3^+$ and ${}_3(0,0)_3^+$ of the ${}^1S^e$ symmetry.] Numbers in square brackets represent powers of ten, e.g., $1[-2]=1\times10^{-2}$.

Z	2	3	4	5
ν	1.92[−2]	3.30[−2]	4.73[−2]	6.17[−2]
ν/Z	0.96[−2]	1.10[−2]	1.18[−2]	1.23[−2]

C. The T doubling

To complete our discussion of moleculelike normal modes, we wish to comment on the T doubling (also referred to as l doubling or Λ doubling). We have already indicated the general tendency for a pair of intrashell states with the same A, L, K, and T but different η (i.e., T doublets) to have $\eta=+$ higher than $\eta=-$. This behavior can be explained in terms of the restriction on each member of the pair of the possible atomic configurations. To demonstrate this, let us consider the He ($N=2$, ${}^1P^o,{}^3P^e$) doublets. The available intrashell configurations are $2s2p$ for ${}^1P^o$ and $2p^2$ for ${}^3P^e$. Let us set $\alpha=\pi/4$. Then the antisymmetrized wave function of the former is proportional to the M component of the vector or $(\hat{\mathbf{r}}_1+\hat{\mathbf{r}}_2)$ [proportional to $\mathcal{Y}_{011M}(\hat{\mathbf{r}}_1,\hat{\mathbf{r}}_2)+\mathcal{Y}_{011M}(\hat{\mathbf{r}}_2,\hat{\mathbf{r}}_1)$]. Similarly, the wave function of the latter is proportional to the M component of the vector $\hat{\mathbf{r}}_1\times\hat{\mathbf{r}}_2$. Their densities are proportional to $1+\cos\theta_{12}$ and $\sin^2\theta_{12}$, respectively. Since $\sin^2\theta_{12}$ vanishes at $\theta_{12}=0$, and π, the ${}^3P^e$ intrashell state already has the behavior characterized by $(K,T)=(0,1)$. The formation of a rovibrator mode for the ${}^1P^o$ state requires the configuration interaction with the neighboring intrashell states such as $2s3p,2p3d,2p4d,\ldots$. These states have rather small amplitude near $\alpha=\pi/4$ so that their contribution is somewhat marginal in reducing the amplitude at $\theta_{12}=0$ and in sharpening the rovibrator behavior. Therefore the repulsion is larger for ${}^1P^o$ than for ${}^3P^e$. This argument can be readily generalized to $l_1,l_2>2$ as in Ref. 5 noting the property

$$\mathcal{Y}_{l_1l_2LM}(\hat{\mathbf{r}}_1,\hat{\mathbf{r}}_2)=\eta\mathcal{Y}_{l_2l_1LM}(\hat{\mathbf{r}}_2,\hat{\mathbf{r}}_1) \tag{42}$$

and $\theta_{12}=0$ when $\hat{\mathbf{r}}_1=\hat{\mathbf{r}}_2$. A demonstration of this fact is given in Fig. 11 for a nontrivial case of He ($N=3$, ${}^1F^o,{}^3F^e$) with $(K,\eta T)_N^A=(1,\pm1)_3^+$ by slicing the reduced

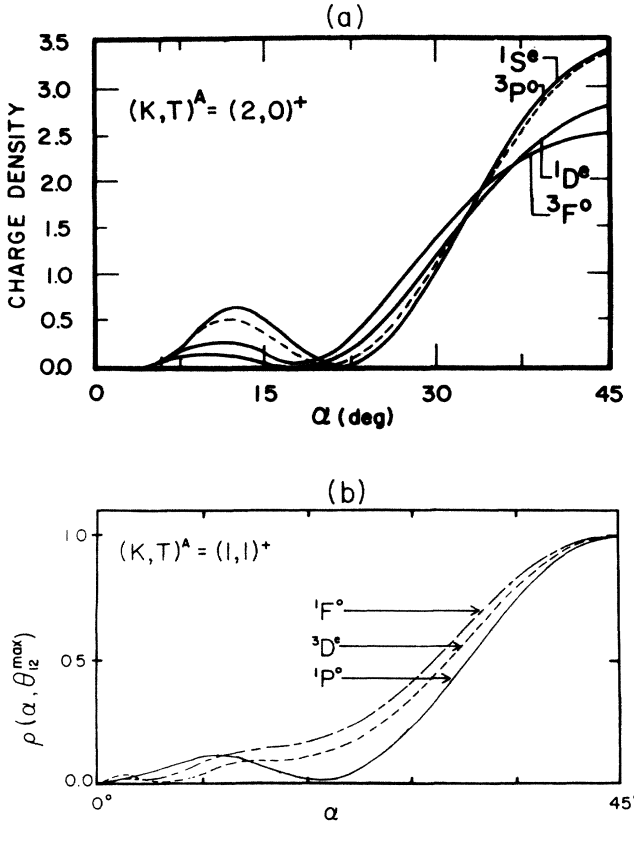

FIG. 9. (a) Sectional view of the charge density as a function of α for channels with $(K,T)^A=(2,0)_3^+$, (b) same for $(K,T)^A=(1,1)_3^+$. In (b), the charge density is renormalized so that the maximum is unity.

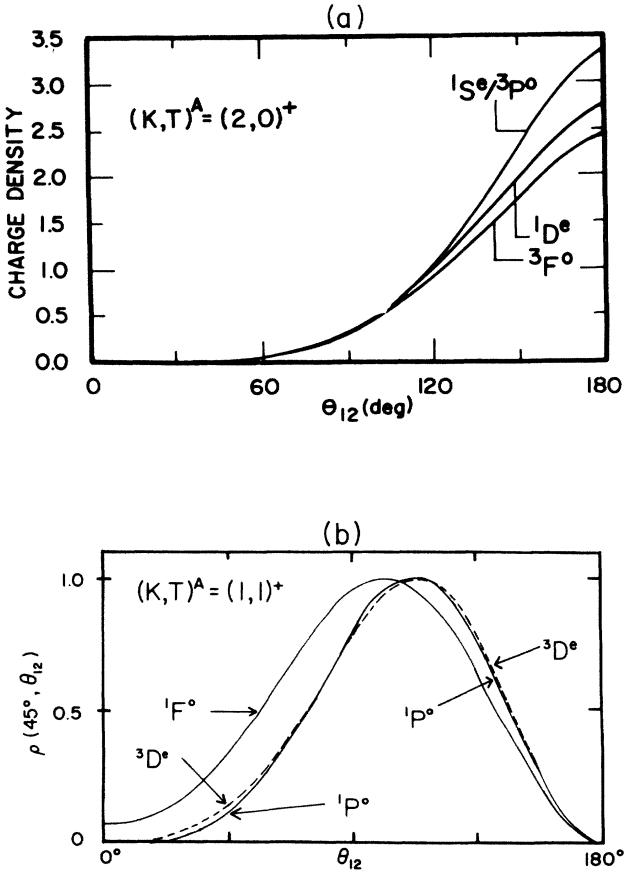

FIG. 10. (a) Sectional view of the charge density as a function of θ_{12} for channels with $(K,T)^A=(2,0)_3^+$ as in Fig. 9(a), (b) same for $(K,T)^A=(1,1)_3^+$ as in Fig. 9(b).

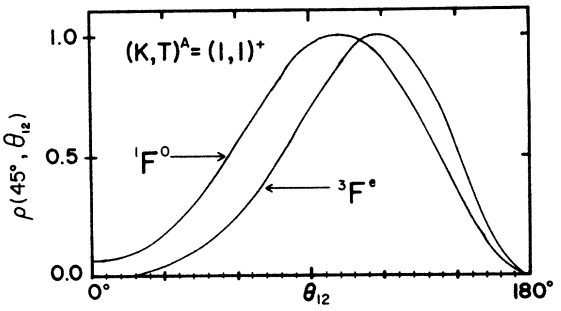

FIG. 11. Demonstration of the nonvanishing amplitude of the $(1,1)_3^+ {}^1F^o$ charge density at $\alpha=\pi/4$, $\theta_{12}=0$. On the contrary, the $(1,1)_3^+ {}^3F^e$ charge density vanishes identically. Angular configurations included are sf,pd,dg,df,fg for $^1F^o$, pf,d^2,f^2,dg,gd for $^3F^e$.

density at $\alpha=\pi/4$ as a function of θ_{12}. Note that the nonvanishing amplitude of $^1F^o$ ($\eta=+1$) at $\theta_{12}=0$ which enlarges the effect of the bielectronic repulsion is responsible for the fact that $^1F^o$ lies slightly above $^3F^e$ (see Fig. 7).

V. SYSTEMATICS OF AUTOIONIZATION WIDTHS

In this section we study whether the knowledge of moleculelike normal modes gives insight into two-electron dynamics. There is fragmentary evidence indicating certain systematics in decay widths, which can be explained qualitatively in terms of molecululelike normal modes. The overlap between the quasibound resonance wave function and a continuum wave function is large near the locus of the ridge[20] where the pair correlation in the continuum channel is just breaking up and the quasibound resonant wave function is gaining amplitude. From the configuration-interaction viewpoint, the major contribution to the overlap weighted by the bielectronic repulsion arises from the $\alpha=\pi/4$, $\theta_{12}=0$ region, and is large when both channels have similar characteristics. The details of the asymptotic portion of the continuum wave function do not matter owing to this localization of the coupling region. Therefore a rule of thumb[3] is that the partial width is the largest when the continuum channel corresponds to

(i) $\Delta N=-1$, $\Delta K=-1$ (i.e., $\Delta v=0$), $\Delta T=0$ with A unchanged. This rule is well satisfied in the e-H collision,[13,23] for example, other rules which follow from similar arguments are the following:

(ii) The $-$ states have widths that are orders of magnitudes smaller than those of the corresponding $+$ states because of both the reduction in amplitude near $\alpha=\pi/4,\theta_{12}=0$ and also of the expanded size of the atomic states which makes the amplitude of the wave function small at the critical value of R.

(iii) The lower member of a T doublet generally has the smaller width since it has the less amplitude near $\alpha=\pi/4$, $\theta_{12}=0$ (Sec. IV C).

(iv) When N, T, and K are the same then the states with higher L have larger widths. This is because the higher rotor states have larger amplitude near $\theta_{12}=0$ (see Table V). However, this effect is more subtle since higher L states have less amplitude near $\alpha=\pi/4$ (Sec. III B). When the former factor is dominant, which appears to be often the case, then this rule applies.

(v) When N, L, S, π, and K are the same, then the ones with the larger T have the larger widths. This is due to the increase in the amplitude near $\theta_{12}=0$. [For example, the $_3(0,0)_3^+ {}^1D^e$ state is narrower than the $_3(0,2)_3^+ {}^1D^e$ state by factor 3.5.][13]

(vi) When N, L, S, π, and T are the same, then the one with smaller v is expected to be narrower since the larger v is the larger the amplitude near $\theta_{12}=0$. [For example, the $_3(2,0)_3^+ {}^1S^e$ state is narrower than the $_3(0,0)_3^+ {}^1S^e$ state by a factor of 1.8.] However, for the majority of cases, the increase of v leads to a considerable reduction in correlation energy and hence to the significant shallowing of the potential well. The radial wave function then extends further out and the normalization integral is dictated by the large R contribution, resulting in the reduction of the amplitude at small R. This inverts the trend. Typical examples of this inversion are the pairs $_3(0,0)_3^+$ and $_3(2,0)_3^+$ of $^3P^o$ and $^1D^e$, and $_3(-1,1)_3^+$,$_3(1,1)_3^+$ of $^1P^o$. The ratios of the widths[13] are 2.0, 7.4, 2.2, respectively.

We note that the rules (i), (ii), and (iii) have rather general validity but the others arise from a few competing effects, so exceptions occur. These rules were drawn from data in the presently available literature. Confirmation of these rules must be based on more accurate and extensive compilation of widths and on critical analysis of competing effects. In the future, efforts should be directed to this end.

VI. CONCLUSIONS

In this article we examined the wave functions calculated in hyperspherical coordinates in the body frame of the atom. By decomposing the body-frame wave functions into rotational components, the quantum numbers K, T,

TABLE V. This set of data demonstrates how width grows along the rotor series owing to the increases in the amplitude near $\theta_{12}=0$. Numbers in square brackets represent powers of ten, e.g., $1[-2]=1\times10^{-2}$.

$_n(K,T)_N^{A\,2S+1}L^\pi$	Width (eV)	
He**		
$_3(2,0)_3^+ {}^1S^e$	0.828[−1][a]	0.825[−1][b]
$^3P^o$	0.976[−1][a]	0.116[b]
$^1D^e$	0.242[a]	0.154[b]
$(H^-)^{**}$		
$_3(2,0)_3^+ {}^1S^e$	0.388[−1][c]	
$^3P^o$	0.483[−1][c]	
$^1D^e$	0.493[−1][c]	
$_5(4,0)_5^+ {}^1S^e$	0.150[−1][d]	
$^3P^o$	0.163[−1][d]	
$^1D^e$	0.177[−1][d]	

[a]Reference 13.
[b]Reference 24.
[c]Reference 25.
[d]Reference 26(a).

and A used by Lin for the classification of doubly excited states were related to the moleculelike behavior of the atom. The framework developed permits us to have a very global and unified picture of two-electron correlations: Not only the classification scheme based on hyperspherical coordinates can be qualitatively related to the rovibrator model and its quantum numbers, but the quantitative deviations of molecular term constants from the latter model can be assessed.

The picture presented here in part parallels that of the group-theoretical treatment and in part complements it. Examination of the wave function calculated in hyperspherical coordinates in the body frame of the atom allows the immediate interpretation of rovibrational quantum numbers and the quantum numbers K and T obtained in the O(4) scheme; it also allows the identification of radial quantum number A directly. Thus, the approximate symmetries which are implicit in the labeling of energy levels are identified with pictures of coupled electron motions, either in terms of the pattern of radial and angular correlations or in terms of the qualitative molecular normal modes.

The body-frame analysis elucidates the underlying correlations with emphasis on the geometrical constraints of the wave function of the system. The systematics inferred from the study of quasi-invariants are considerably sharpened in the hyperspherical analysis.

Despite the unified view of doubly excited states developed in this paper, there still remain a number of open questions: How should the normal modes of doubly excited states formed by two valence electrons be affected by the presence of a structured core? How should the moleculelike normal modes manifest themselves in angular distribution of fragments, for example? (A partial answer was given by Greene,[11] but a global picture is still lacking.) How does the structure theory presented here help us in understanding the dynamical aspects of collisions (such as the formation of He^{**} in $He^{+}+He$ collisions[27])? As a further extension, we may ask ourselves whether triply excited states exhibit XY_3 moleculelike normal modes. We hope that in the future these questions will be studied both experimentally and theoretically.

ACKNOWLEDGMENTS

We wish to acknowledge useful discussion with U. Fano and M. Le Dourneuf on this subject. One of us (S.W.) was supported in part by the Centre National de la Recherche Scientifique (CNRS) at the Paris observatory at Meudon and in part by the NATO Grant No. 328. One of us (C.D.L.) was supported in part by the U.S. Department of Energy, Division of Chemical Sciences. This project was also supported by the National Science Foundation-CNRS international cooperative research program.

APPENDIX A: SYMMETRY PROPERTIES OF THE BODY-FRAME FUNCTION Ψ^L_Q UNDER PARTICLE EXCHANGE AND REFLECTION WITH RESPECT TO $\theta_{12}=\pi$

In this appendix we derive the symmetry properties of $\psi^L_Q(R,\alpha,\theta_{12})$ under (i) $\alpha\to\pi/2-\alpha$ and (ii) $\theta_{12}\to 2\pi-\theta_{12}$. The final results were given in Eqs. (13) and (17), respectively.

Under the exchange of particles 1 and 2, $\alpha\to\pi/2-\alpha$ and $\chi\to\pi-(\chi+\theta_{12})$. (See Fig. 2.) According to our choice of the body frame, the new coordinate system is $(\hat{\mathbf{s}},-\hat{\mathbf{t}},-\hat{\mathbf{r}}_{12})$. In the new frame,

$$\hat{\mathbf{r}}_1''=(\pi-(\chi+\theta_{12}),0)\ , \tag{A1}$$

$$\hat{\mathbf{r}}_2''=(\pi-\chi,0)\ , \tag{A2}$$

and the body-frame function (12) is given by

$$\psi^L_Q\left[R,\frac{\pi}{2}-\alpha,\theta_{12}\right]=\sum_{l_1,l_2}\psi^L_{l_1l_2}(R\sin\alpha,R\cos\alpha)\times\mathcal{Y}_{l_1l_2LQ}(\hat{\mathbf{r}}_1'',\hat{\mathbf{r}}_2'')\ . \tag{A3}$$

From the following relations,

$$Y_{lm}(\pi-\theta,\pi+\phi)=(-1)^lY_{lm}(\theta,\phi) \tag{A4}$$

and

$$Y_{lm}(\pi-\theta,\pi)=(-1)^mY_{lm}(\pi-\theta,0)\ , \tag{A5}$$

we obtain

$$Y_{lm}(\pi-\theta,0)=(-1)^{l+m}Y_{lm}(\theta,0) \tag{A6}$$

such that

$$\begin{aligned}\mathcal{Y}_{l_1l_2LQ}(\hat{\mathbf{r}}_1'',\hat{\mathbf{r}}_2'')&=\sum_{m_1,m_2}\langle l_1m_1l_2m_2\,|\,LQ\rangle Y_{l_1m_1}(\hat{\mathbf{r}}_1'')Y_{l_2l_2}(\hat{\mathbf{r}}_2'')\\&=\sum_{m_1,m_2}\langle l_1m_1l_2m_2\,|\,LQ\rangle Y_{l_1m_1}(\pi-(\chi+\theta_{12}),0)Y_{l_2m_2}(\pi-\chi,0)\\&=\sum_{m_1,m_2}\langle l_1m_1l_2m_2\,|\,LQ\rangle(-1)^{l_1+l_2+Q}Y_{l_1m_1}(\chi+\theta_{12},0)Y_{l_2m_2}(\chi,0)\\&=(-1)^{l_1+l_2+Q}\mathcal{Y}_{l_1l_2LQ}(\hat{\mathbf{r}}_2',\hat{\mathbf{r}}_1')\\&=(-1)^{L+Q}\mathcal{Y}_{l_2l_1LQ}(\hat{\mathbf{r}}_1',\hat{\mathbf{r}}_2')\ ,\end{aligned} \tag{A7}$$

where we have used

$$\mathscr{Y}_{l_1 l_2 LQ}(\hat{\mathbf{r}}_2,\hat{\mathbf{r}}_1)=(-1)^{l_1+l_2+L}\mathscr{Y}_{l_2 l_1 LQ}(\hat{\mathbf{r}}_1,\hat{\mathbf{r}}_2) \tag{A8}$$

and $Q=m_1+m_2$.

We also need to know $\psi^L_{l_1 l_2}(r_2,r_1)$. From Eq. (10),

$$\psi(\mathbf{r}_2,\mathbf{r}_1)=\sum_{l_1 l_2}\psi^L_{l_1 l_2}(r_2,r_1)\mathscr{Y}_{l_1 l_2 LM}(\hat{\mathbf{r}}_2,\hat{\mathbf{r}}_1) \tag{A9}$$

$$=(-1)^S\psi(\mathbf{r}_1,\mathbf{r}_2) \tag{A10}$$

$$=(-1)^S\sum_{l_1,l_2}\psi^L_{l_1 l_2}(r_1,r_2)\mathscr{Y}_{l_1 l_2 LM}(\hat{\mathbf{r}}_1,\hat{\mathbf{r}}_2)\ . \tag{A11}$$

We can see easily that

$$\psi^L_{l_1 l_2}(r_2,r_1)=(-1)^{l_1+l_2+L+S}\psi^L_{l_2 l_1}(r_1,r_2)\ . \tag{A12}$$

With Eqs. (A8) and (A12), Eq. (A3) reduces to

$$\psi^L_Q\left[R,\frac{\pi}{2}-\alpha,\theta_{12}\right]=\sum_{l_1 l_2}\psi^L_{l_1 l_2}(r_2,r_1)\mathscr{Y}_{l_1 l_2 LQ}(\hat{\mathbf{r}}''_1,\hat{\mathbf{r}}''_2)$$

$$=\sum_{l_1,l_2}(-1)^{l_1+l_2+L+S}\psi^L_{l_2 l_1}(r_1,r_2)\mathscr{Y}_{l_2 l_1 LQ}(\hat{\mathbf{r}}'_1,\hat{\mathbf{r}}'_2)(-1)^{L+Q}$$

$$=\pi(-1)^{S+Q}\psi^L_Q(R,\alpha,\theta_{12})\ , \tag{A13}$$

where π is the parity of the state. This is the result given in (13). Notice that the change of frame $(\hat{\mathbf{s}},\hat{\mathbf{t}},\hat{\mathbf{r}}_{12})\rightarrow(\hat{\mathbf{s}},-\hat{\mathbf{t}},-\hat{\mathbf{r}}_{12})$ is equivalent to the rotation about the $\hat{s}$ axis through π. This transforms $D^{(L)}_{QM}\rightarrow(-1)^L D^{(L)}_{-QM}$. Combining with Eqs. (15) and (A13), one also sees that the spatial wave function indeed gains the phase factor $(-1)^S$ as in Eq. (A10).

To derive (17), we notice that the reflection with respect to $\theta_{12}=\pi$ axis is equivalent to the replacement of $\chi\rightarrow-\chi$, and $\chi+\theta_{12}\rightarrow2\pi-(\chi+\theta_{12})$. Using the property

$$Y_{lm}(-\theta,0)=(-1)^m Y_{lm}(\theta,0) \tag{A14}$$

it is easily seen that

$$\psi^L_Q(R,\alpha,2\pi-\theta_{12})=(-1)^Q\psi^L_Q(R,\alpha,\theta_{12})\ , \tag{A15}$$

which is identical to Eq. (17).

[1](a) M. E. Kellman and D. R. Herrick, Phys. Rev. A **22**, 1536 (1980); (b) J. Phys. B **11**, L755 (1978).

[2]D. R. Herrick, M. E. Kellman, and R. D. Poliak, Phys. Rev. A **22**, 1517 (1980).

[3]D. R. Herrick, Adv. Chem. Phys. **52**, 1 (1983).

[4]P. Rehmus and R. S. Berry, Chem. Phys. **38**, 257 (1979).

[5]G. S. Ezra and R. S. Berry, Phys. Rev. A **28**, 1974 (1983). See Also H. J. Yuh, G. Ezra, P. Rehmus and R. S. Berry, Phys. Rev. Lett. **47**, 497 (1981).

[6]P. R. Bunker and J. M. R. Stone, J. Mol. Spectrosc. **41**, 310 (1972).

[7](a) C. D. Lin, Phys. Rev. A **25**, 76 (1982); (b) **26**, 2305 (1982); (c) **27**, 22 (1983); **25**, 1535 (1982); (d) **29**, 1019 (1984).

[8]J. H. Macek, J. Phys. B **1**, 831 (1968).

[9]U. Fano, Rep. Prog. Phys. **46**, 97 (1983), and references therein.

[10]H. Klar and W. Schlecht, J. Phys. B **9**, 7699 (1976).

[11]C. H. Greene, Phys. Rev. Lett. **44**, 869 (1980).

[12]C. Wulfman, Chem. Phys. Lett. **23**, 370 (1973).

[13]D. R. Herrick and O. Sinanoglu, Phys. Rev. A **11**, 97 (1975).

[14]J. D. Louck and H. W. Galbraith, Rev. Mod. Phys. **48**, 69 (1976).

[15]E. A. Solovev, Zh. Eksp. Teor. Fiz. **82**, 1762 (1982) [Sov. Phys.—JETP **55**, 1017 (1982)].

[16]D. R. Herrick, Phys. Rev. A **12**, 413 (1975).

[17]E. Thiele and D. J. Wilson, J. Chem. Phys. **35**, 1256 (1961).

[18]J. M. Launay and M. L. Dourneuf, J. Phys. B **15**, L455 (1982).

[19](a) M. J. Davis and E. J. Heller, J. Chem. Phys. **75**, 246 (1981); (b) **73**, 4720 (1980).

[20]U. Fano, Phys. Rev. A **24**, 2402 (1981).

[21]A. R. P. Rau, Phys. Rev. A **4**, 207 (1971).

[22]L. Lipsky, R. Anania, and M. J. Corneely, At. Data Nucl. Data Tables **20**, 727 (1977).

[23]J. Macek and P. G. Burke, Proc. Phys. Soc. London **92**, 351 (1967).

[24]P. G. Burke and A. J. Taylor, J. Phys. B **2**, 44 (1969).

[25]P. G. Burke, *Advances in Atomic and Molecular Physics*, edited by D. R. Bates and I. Esterman (Academic, New York, 1968), Vol. 4, pp. 173–249.

[26](a) Y. K. Ho and J. Callaway, Phys. Rev. A **27**, 1887 (1983); (b) J. Phys. B **17**, L559 (1984).

[27](a) J. M. Feagin, J. S. Briggs and T. M. Reeves, J. Phys. B **17**, 1057 (1984); (b) A. Itoh, T. J. M. Zouros, D. Schneider, U. Stettner, W. Zeitz, and N. Stolterfoht, *ibid.* (to be published).